Inorganic Chemistry
Article

Inorg. Chem. 2010, 49, 29–37 29
DOI: 10.1021/ic9008015

Dynamics and Equilibrium of Heme Axial Ligation in Mesoporous Nanocrystalline TiO_2 Thin Films

Amanda J. Morris, Jonathan R. Stromberg, and Gerald J. Meyer*

Departments of Chemistry and Materials Science and Engineering, Johns Hopkins University, 3400 North Charles Street, Baltimore, Maryland 21218

Received April 24, 2009

Comparative studies of axial CO and solvent coordination to iron(II) protoporphyrin IX (Fe^{II}PPIX) anchored to the surface of mesoporous nanocrystalline (anatase) TiO_2 thin films (Fe^{II}PPIX/TiO_2) immersed in dimethyl sulfoxide (DMSO), pyridine (py), and methanol (MeOH) and to Fe^{II}PPIX in fluid DMSO and py solution are reported. The equilibrium constants, K^{S}_{eqCO}, for CO coordination to Fe^{II}PPIX/TiO_2 immersed in py (2.4×10^3 M^{-1}) < DMSO (6×10^4 M^{-1}) < MeOH (2.3×10^5 M^{-1}) were quantified. The corresponding values in fluid py or DMSO solution were ~2 times larger (4.5×10^3 and 1×10^5 M^{-1}, respectively). The observed ligand exchange rates (k_{obs}) measured after pulsed 532 nm laser excitation (5−6 ns fwhm, 1−3 mJ/pulse) of (S)(CO)Fe^{II}PPIX/TiO_2, where S is solvent, in saturated CO solutions were measured: py (2.2 s^{-1}), DMSO (460 s^{-1}), MeOH (2.09×10^5 s^{-1}). The corresponding values in fluid solution were 2.0 s^{-1} (py) and 230 s^{-1} (DMSO). The observed ligand exchange rate varied linearly with [CO], and second-order rate constants were determined for Fe^{II}PPIX/TiO_2 immersed in DMSO (3.1×10^5 M^{-1} s^{-1}) and MeOH (1.5×10^7 M^{-1} s^{-1}). The observed rate for CO addition to $(py)_2Fe^{II}$PPIX/TiO_2 immersed in py did not vary linearly with [CO]. The relevance of the measured kinetics and thermodynamics to a dissociative mechanism for ligand exchange is discussed.

Introduction

As global energy consumption continues to rise, there is a pressing need for the production of solar fuels.[1] Molecular approaches to practical solar fuel generation will likely require the integration of (1) light absorption, (2) electron transfer, and (3) catalysis.[2−5] An appealing starting point is with sensitized mesoporous nanocrystalline (anatase) titanium dioxide thin films that have been developed for application in dye-sensitized solar cells.[6,7] These materials already largely satisfy the first two stated requirements, efficient solar harvesting and excited-state electron transfer. Indeed, with Ru(II) polypyridyl compounds, such as *cis*-$Ru(dcb)_2(NCS)_2$, where dcb is 4,4′-$(CO_2H)_2$-bipyridine, nearly quantitative excited-state electron injection into TiO_2 occurs across the visible region (~400−750 nm) on an absorbed photon basis.[8] Furthermore, under some conditions the injected electron can be separated from the "hole" or oxidizing equivalent and quantitatively collected in an external circuit.[9,10] Remaining is the challenge of redox catalysis.

This paper describes fundamental studies of hemes (iron(II) protoporphyrin IX (Fe^{II}PPIX)) anchored to the surface of mesoporous nanocrystalline (anatase) titanium dioxide, Scheme 1). While iron metalloporphyrins may not be useful catalysts for practical solar fuel generation, they do have a number of desirable properties for fundamental studies.[11−13] These include high stability, well-defined spectroscopic properties in adjacent formal oxidation states, and the ability to drive multiple-electron transfer reactions. Indeed, it has been shown that hemes anchored to TiO_2 can undergo two-electron transfer reactions to organohalides that, in some cases, results in the formation of stable carbene compounds.[14,15] Yet another property of hemes that could be

*To whom correspondence should be addressed. E-mail: meyer@jhu.edu.

(1) Lewis, N. S.; Nocera, D. G. *Proc. Natl. Acad. Sci. U.S.A.* **2006**, *103*, 15729.
(2) Alstrum-Acevedo, J. H.; Brennaman, M. K.; Meyer, T. J. *Inorg. Chem.* **2005**, *44*, 6802.
(3) Chakraborty, S.; Wadas, T. J.; Hester, H.; Schmehl, R.; Eisenberg, R. *Inorg. Chem.* **2005**, *44*, 6865.
(4) Dempsey, J. L.; Esswein, A. J.; Manke, D. R.; Rosenthal, J.; Soper, J. D.; Nocera, D. G. *Inorg. Chem.* **2005**, *44*, 6879.
(5) Gust, D.; Moore, T. A.; Moore, A. L. *Acc. Chem. Res.* **2001**, *34*, 40.
(6) O'Regan, B.; Graetzel, M. *Nature* **1991**, *353*, 737.
(7) O'Regan, B.; Moser, J.; Anderson, M.; Graetzel, M. *J. Phys. Chem.* **1990**, *94*, 8720.
(8) Nazeeruddin, M. K.; Kay, A.; Rodicio, I.; Humphry-Baker, R.; Mueller, E.; Liska, P.; Vlachopoulos, N.; Graetzel, M. *J. Am. Chem. Soc.* **1993**, *115*, 6382.
(9) Hagfeldt, A.; Graetzel, M. *Chem. Rev.* **1995**, *95*, 49.
(10) Ardo, S.; Meyer, G. J. *Chem. Soc. Rev.* **2009**, *38*, 115.
(11) Antonini, E.; Brunori, M. *Hemoglobin and Myoglobin in their Reactions with Ligands*; North-Holland: Amsterdam, 1971; Frontiers of Biology, Vol. *21*.
(12) Scheidt, W. R.; Reed, C. A. *Chem. Rev.* **1981**, *81*, 543.
(13) Momenteau, M.; Reed, C. A. *Chem. Rev.* **1994**, *94*, 659.
(14) Obare, S. O.; Ito, T.; Meyer, G. J. *J. Am. Chem. Soc.* **2006**, *128*, 712.
(15) Stromberg, J. R.; Wnuk, J. D.; Pinlac, R. A. F.; Meyer, G. J. *Nano Lett.* **2006**, *6*, 1284.

Published on Web 12/07/2009

Scheme 1. Iron(II) Protoporphyrin IX (Fe^{II}PPIX) Anchored to the Surface of Mesoporous Nanocrystalline (Anatase) Titanium Dioxide

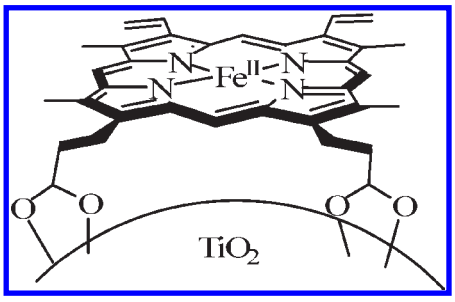

exploited for fundamental catalysis studies at semiconductor interfaces is axial ligand coordination to tune reactivity.[16−19]

The goals of this paper were to (1) quantify the influence of the mesoporous TiO_2 film on the thermodynamics and kinetics of axial ligand exchange and (2) understand the influence of illumination on excited-state electron transfer and/or ligand exchange. To this end, comparative experiments were conducted with Fe^{II}PPIX anchored to the surface of TiO_2 and in fluid solution that revealed a significant environmental dependence on the kinetic parameters which define ligand equilibrium.

Experimental Section

Materials. Methanol (MeOH; Aldrich, >99.9%), pyridine (py; Fisher, ACS), hemin (iron(III) protoporphyrin chloride, $ClFe^{III}$PPIX; Fluka, 98.0%), dimethyl sulfoxide (DMSO; Fisher, ACS), and sodium hydrosulfite (Aldrich, ~85%) were used as received.

Preparation of $(DMSO)_2Fe^{II}$PPIX and (DMSO)(CO)Fe^{II}PPIX. Samples were prepared by a method that has previously been described, save for the transfer of the $(DMSO)_2Fe^{II}$PPIX solution via a cannula to a cuvette free of excess dithionite.[17]

Preparation of $(py)_2Fe^{II}$PPIX and (py)(CO)Fe^{II}PPIX. Samples were prepared by methods that have previously been described, save for the elimination of excess base and the phosphate buffer in the reducing solution.[17,20]

TiO_2 Thin Films. Mesoporous thin films (10 μm thick) of ~20 nm anatase TiO_2 nanocrystallites were prepared by a sol−gel technique that has been previously described.[21] Freshly prepared films were soaked in a concentrated DMSO solution of hemin for ~5 min until the desired surface coverage was reached. These films were then washed with MeOH, py, or DMSO and used. The hemin/TiO_2 films were placed into cuvettes of neat MeOH, py, or DMSO, purged with Ar gas for at least 30 min, and photolyzed with UV light (>320 nm) to yield heme/TiO_2 (Fe^{II}PPIX/TiO_2). Samples were then purged with carbon monoxide or a carbon monoxide/nitrogen mix for 5−30 min.

Gas Mixing. Carbon monoxide (Airgas, CP grade) and/or a custom CO-in-N_2 gas mixture (Airgas) were mixed with nitrogen (Airgas, ultrahigh-purity grade) through two MKS Instruments mass flow controllers (MFCs, MKS 1179A) controlled by an MKS Instruments Multi Gas Controller (MGC, MKS 647C). The MFCs have a maximum flow rate of 200 standard cubic centimeters per minute (sccm). The gas composition was controlled by the set flow rates of the gases. For example, a 10% CO mixture was made by mixing CO at a flow rate of 20 sccm with N_2 at 180 sccm. The concentration of CO in solution was determined from a Henry's law relation

$$K_H = \frac{P_{CO}}{[CO]} \quad (1)$$

using known CO solubilities in DMSO (1.1 mM), py (4.79 mM), and MeOH (10.8 mM).[22,23]

Absorbance Measurements. Steady-state UV−vis absorbance measurements were made on a Cary 14 spectrophotometer. The TiO_2 thin films were placed diagonally in the cuvette with the solvent of interest. An unsensitized TiO_2 thin film in the solvent of interest was used as a reference.

FTIR. Solution infrared spectra were obtained in a Spectralys Specac solution IR cell with a 2 mm path length and fitted with KBr windows at room temperature with a Nexus 670 Thermo-Nicolet FTIR spectrometer. The data collected were an average of 64 scans with 2 cm^{-1} resolution. The C−O stretching frequencies for (DMSO)(CO)Fe^{II}PPIX and (py)(CO)Fe^{II}PPIX were 1942 and 1959 cm^{-1}, respectively. Solution spectra of (MeOH)(CO)Fe^{II}PPIX were not collected, due to the insolubility of Fe^{III}PPIX in MeOH.

Transient Absorption Spectroscopy. The experimental apparatus was the same as that previously described, except for the replacement of the Continuum Surelite II with a Quantel Brilliant B Nd:YAG laser (λ = 532 nm, fwhm 5−6 ns, 1−3 mJ/pulse) as the excitation source. A 150 W Xe lamp was used as the probe beam and was pulsed for short (<10 μs) time scale measurements. The sample was protected from probe light using long-pass glass filters. Transient absorption changes were monitored every 2 nm and typically represent the average of 45 laser shots.

The relative quantum yields for the photorelease of CO were quantified by comparative actinometry on a 10 ns time scale. A (MeOH)(CO)Fe^{II}PPIX/TiO_2 thin film was used as the actinometer, and the yield of CO release was defined as 1. The absorbance of all other TiO_2 thin film samples was approximately matched at the excitation wavelength, 532 nm.

Results

Steady-State Spectroscopy. Mesoporous nanocrystalline (anatase) thin films were prepared by a sol−gel method that has previously been described.[21] The materials were functionalized with hemin by room-temperature reactions in dimethyl sulfoxide (DMSO), abbreviated $(DMSO)_2Fe^{III}$PPIX/TiO_2. Band-gap excitation of the thin films immersed in Ar-purged solvent resulted in the reduction of Fe^{III} to Fe^{II} and a bathochromic shift in the Soret band for all ligations (Figure 1 and Table 1).[24] In the ferrous state, the axial ligands were identified clearly as DMSO or py by examination of the Q-band region of the visible absorption spectrum.[20,25−27] The

(16) El-Kasmi, D.; Tetreau, C.; Lavalette, D.; Momenteau, M. *J. Am. Chem. Soc.* **1995**, *117*, 6041.
(17) Larsen, R. W.; Murphy, J.; Findsen, E. W. *Inorg. Chem.* **1996**, *35*, 6254.
(18) Lavalette, D.; Tetreau, C.; Momenteau, M. *J. Am. Chem. Soc.* **1979**, *101*, 5395.
(19) Thompson, D. W.; Kretzer, R. M.; Lebeau, E. L.; Scaltrito, D. V.; Ghiladi, R. A.; Lam, K.-C.; Rheingold, A. L.; Karlin, K. D.; Meyer, G. J. *Inorg. Chem.* **2003**, *42*, 5211.
(20) Winterhalter, K. H.; Ioppolo, C.; Antonini, E. *Biochemistry* **1971**, *10*, 3790.
(21) Heimer, T. A.; D'Arcangelis, S. T.; Farzad, F.; Stipkala, J. M.; Meyer, G. J. *Inorg. Chem.* **1996**, *35*, 5319.
(22) Ercolani, C.; Monacelli, F.; Pennesi, G.; Rossi, G.; Antonini, E.; Ascenzi, P.; Brunori, M. *J. Chem. Soc., Dalton Trans.* **1981**, 1120.
(23) Ohlin, C. A.; Dyson, P. J.; Laurenczy, G. *Chem. Commun.* **2004**, 1070.
(24) Obare, S. O.; Ito, T.; Balfour, M. H.; Meyer, G. J. *Nano Lett.* **2003**, *3*, 1151.
(25) Larsen, R. W.; Findsen, E. W.; Nalliah, R. E. *Inorg. Chim. Acta* **1995**, *234*, 101.
(26) Obare, S. O.; Ito, T.; Meyer, G. J. *Environ. Sci. Technol.* **2005**, *39*, 6266.
(27) Nalliah, R. E.; Findsen, E. W. *J. Raman Spectrosc.* **1993**, *24*, 867.

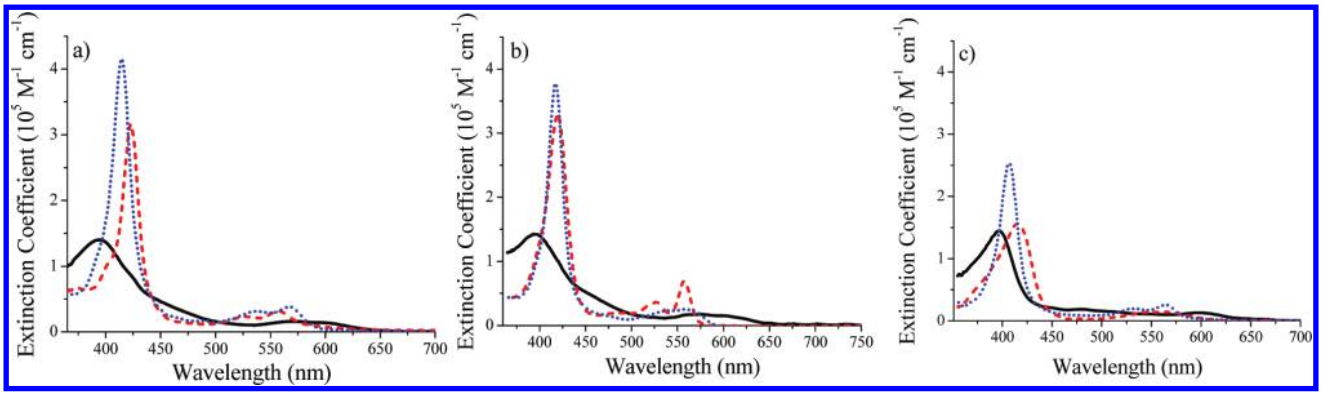

Figure 1. Absorbance spectra of (a) $(DMSO)_2Fe^{III}PPIX/TiO_2$ (black solid line), $(DMSO)_2Fe^{II}PPIX/TiO_2$ (red dashed line), and $(DMSO)(CO)Fe^{II}PPIX/TiO_2$ (blue dotted line) in DMSO, (b) $(py)_2Fe^{III}PPIX/TiO_2$ (black solid line), $(py)_2Fe^{II}PPIX/TiO_2$ (red dashed line), and $(py)(CO)Fe^{II}PPIX/TiO_2$ (blue dotted line) in py, and (c) $(MeOH)_2Fe^{III}PPIX/TiO_2$ (black solid line), $(MeOH)_2Fe^{II}PPIX/TiO_2$ (red dashed line), and $(MeOH)(CO)Fe^{II}PPIX/TiO_2$ (blue dotted line) in MeOH.

Table 1. Spectral Data for Fe^{III} and Fe^{II} PPIX in Fluid Solution and Anchored to Nanocrystalline TiO_2 Thin Films Immersed in the Same Solvent

solvent		complex								
		$[(S)_2Fe^{III}PPIX]^+$			$(S)_2Fe^{II}PPIX$			$(S)(CO)Fe^{II}PPIX$		
		Soret (nm) [ε (M^{-1} cm^{-1})][a]	β-band (nm)	α-band (nm)	Soret (nm) [ε (M^{-1} cm^{-1})][a]	β-band (nm)	α-band (nm)	Soret (nm) [ε (M^{-1} cm^{-1})][a]	β-band (nm)	α-band (nm)
DMSO	solution	403	498	624	424	525	557	415	534	568
	TiO_2	394 [1.40×10^5]	535−660[b]		423 [3.16×10^5]	528	556	414 [4.15×10^5]	538	568
pyridine	solution				419	525	556	418	501−594[b]	
	TiO_2	395 [1.42×10^5]	535−660[b]		419 [3.3×10^5]	526	557	417 [3.78×10^5]	498−610[b]	
methanol	TiO_2	396 [1.45×10^5]	480	600	416 [1.56×10^5]	495−625[b]		406 [2.53×10^5]	533	565

[a] Extinction coefficients for $(S)_2Fe^{III}PPIX$ were calculated via Beer's law and were assumed to be unchanged on the TiO_2 surface. Extinction coefficients for $(S)_2Fe^{II}PPIX/TiO_2$ and $(S)(CO)Fe^{II}PPIX/TiO_2$ were based on quantitative photochemical conversion and/or ligand exchange. [b] Broad indistinguishable absorption bands over the indicated wavelength range.

axial ligands for thin films immersed in methanol are unknown but for consistency are referred to as $(MeOH)_2Fe^{III/II}PPIX/TiO_2$.

Carbon Monoxide Equilibrium Binding Constants. The equilibrium binding constants, K^S_{eqCO}, were calculated from the known concentrations of the CO-ligated and solvato compounds and the CO concentration (eq 2 and Scheme 2). The equilibrium constants were obtained as the external solution was purged with a carbon monoxide/nitrogen mix while maintaining an overall pressure of 1 atm. The partial pressure of CO, P_{CO}, was varied, and the [CO] in solution was determined by a Henry's law relation based on known solubilities (eq 2, Experimental Section).[22,23]

$$K^S_{eqCO} = \frac{[(S)(CO)Fe^{II}PPIX]}{[(S)_2Fe^{II}PPIX][CO]} \qquad (2)$$

Figure 2 shows the spectral changes of $(py)_2Fe^{II}PPIX/TiO_2$ that occurred with increased [CO] ($(0-4.6) \times 10^{-3}$ M) in the surrounding py solution. As the [CO] was raised, the absorption due to $(py)_2Fe^{II}PPIX/TiO_2$ decreased concurrently with an increase in absorption due to $(py)(CO)Fe^{II}PPIX/TiO_2$. Isosbestic points were observed at 422, 532, 546, and 565 nm, and the final spectrum obtained indicated complete conversion to $(py)(CO)Fe^{II}PPIX/TiO_2$. The relative concentrations of $(py)_2Fe^{II}PPIX/TiO_2$ and $(py)(CO)Fe^{II}PPIX/TiO_2$ were calculated by deconvolution of the composite spectra. The $[(py)(CO)Fe^{II}PPIX/TiO_2]/[(py)_2Fe^{II}PPIX/TiO_2]$ ratio as a function of CO concentration is shown as an inset in Figure 2. The slope provided the equilibrium constant (Table 2). The same procedure was repeated with MeOH or DMSO in place of pyridine (Figure 2 inset).

Nanosecond Transient Absorption Measurements. Nanosecond transient absorption spectra obtained after pulsed 532 nm excitation of $(DMSO)_2Fe^{II}PPIX$ and $(DMSO)_2Fe^{II}PPIX/TiO_2$ in DMSO were, within experimental error, the same (Figure 3). The spectra showed positive ΔA features below 419 nm and above 430 nm, as well as a bleach in the region between these values. The normalized spectra did not change as a function of time, indicative of one compound being formed. Single-exponential decays were observed both in solution and for the compound anchored to the mesoporous thin film. The first-order kinetic rate constant for regeneration of $(DMSO)_2Fe^{II}PPIX$ was corrected for the DMSO concentration, 14.1 M, yielding a second-order rate constant of $[1.9(0.2)] \times 10^5$ M^{-1} s^{-1}, which agrees well with the literature value.[17] The second-order kinetic rate constant for $(DMSO)_2Fe^{II}PPIX/TiO_2$ calculated in a similar manner was $[9.6(0.2)] \times 10^4$ M^{-1} s^{-1}. Normalized single-wavelength absorption changes for solution and surface data with overlaid first-order fits are presented in the inset of Figure 3. No transient absorbance change was observed after pulsed laser excitation of $(py)_2Fe^{II}PPIX$ or $(MeOH)_2Fe^{II}PPIX$ in solution. Pulsed laser excitation (>3 mJ/pulse) of $(py)_2Fe^{II}PPIX/TiO_2$ or $(MeOH)_2Fe^{II}PPIX/TiO_2$ resulted in very small transient signals, <0.001, that could not be modeled by simple ligand loss.

Scheme 2. Equilibrium Binding of CO to $(S)_2Fe^{II}PPIX/TiO_2$, Where S = Solvent (DMSO, py, MeOH)

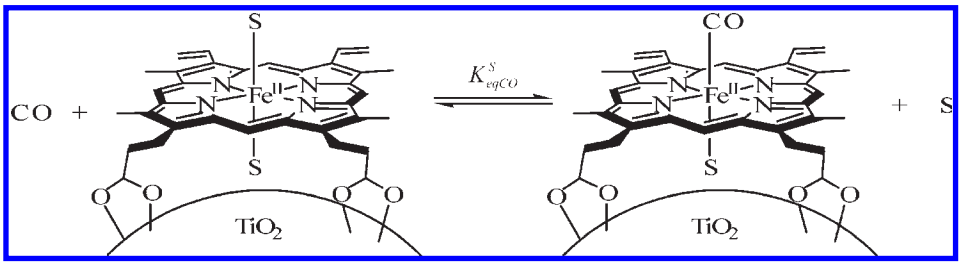

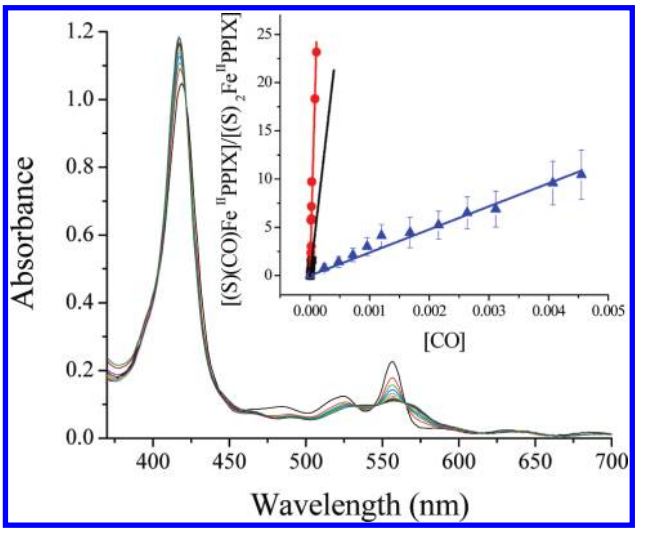

Figure 2. Absorption spectra of $(py)_2Fe^{II}PPIX/TiO_2$ in pyridine with 0, 2.4×10^{-4}, 4.8×10^{-4}, 7.2×10^{-4}, 9.6×10^{-4}, 1.2×10^{-3}, 1.7×10^{-3}, 2.6×10^{-3}, 3.1×10^{-3}, 4.1×10^{-3}, and 4.6×10^{-3} M [CO]. The inset shows plots of the $[(S)(CO)Fe^{II}PPIX/TiO_2]/[(S)_2Fe^{II}PPIX/TiO_2]$ ratio for $(MeOH)_2Fe^{II}PPIX/TiO_2$ in MeOH (red circles), $(DMSO)_2Fe^{II}PPIX/TiO_2$ in DMSO (black squares), $(py)_2Fe^{II}PPIX/TiO_2$ in py (blue triangles) as a function of CO concentration. Error bars indicate 1 standard deviation.

Further experiments will be conducted to investigate the origin of these very weak spectral features.

The absorption difference spectra obtained after pulsed laser excitation of $(MeOH)(CO)Fe^{II}PPIX/TiO_2$ exhibited a bleach from 405 to 416 nm and a positive ΔA feature from 416 to 450 nm (Figure 4). The spectra were modeled as the difference between the absorption spectrum of $(MeOH)(CO)Fe^{II}PPIX/TiO_2$ and $(MeOH)_2Fe^{II}PPIX/TiO_2$. The absorption changes were single-exponential and were independent of the monitoring wavelength over the entire spectral range studied (Figure 4 inset). The decay rate at saturated [CO], k_{obs}, referred to as the observed ligand exchange rate,[28] was $[2.09(0.04)] \times 10^5\ s^{-1}$ (Table 2).

The absorption difference spectrum observed after pulsed laser excitation of $(py)(CO)Fe^{II}PPIX/TiO_2$ in pyridine solution exhibited a bleach from 405 to 424 nm and a growth at longer wavelengths that was, within experimental error, the same as that measured after photoexcitation of $(py)(CO)Fe^{II}PPIX$ in pyridine solution. The spectra were modeled as the difference of the absorption spectra of $(py)(CO)Fe^{II}PPIX/TiO_2$ and $(py)_2Fe^{II}PPIX/TiO_2$. Single-wavelength absorption changes collected at saturated [CO] were not consistent with a first-order kinetic model. The time-resolved data were satisfactorily fit to the Kohlrausch−Williams−Watts (KWW) model, where β is inversely related to a Levy distribution of rate constants, $0 < \beta < 1$ (eq 3):[29]

$$I(t) = I_0 \exp[-(kt)^{\beta}] \quad (3)$$

An average rate constant, $\langle k_{KWW} \rangle$, was calculated as the first moment of the KWW function (eq 4):[30]

$$\langle k_{KWW} \rangle = \frac{k}{\beta}\Gamma\left(\frac{1}{\beta}\right) \quad (4)$$

In pyridine, $\langle k_{KWW} \rangle = 2.2 \pm 0.3\ s^{-1}$ with $\beta = 0.68 \pm 0.03$. Single-wavelength kinetics for $(py)(CO)Fe^{II}PPIX$ in fluid pyridine solution exhibited first-order behavior with an observed ligand exchange rate of 2.0(0.2) s^{-1}.

Two intermediates were observed transiently after pulsed laser excitation of $(DMSO)(CO)Fe^{II}PPIX$ or $(DMSO)(CO)Fe^{II}PPIX/TiO_2$ in DMSO.[31] The first intermediate was observed immediately after the laser pulse, and the second was formed within 4.5 μs (Figure 5 inset). The first intermediate had an absorbance maximum at 437 nm (Figure 5). The identity of the first intermediate was elucidated by comparison with the transient spectrum observed after pulsed laser excitation of $(DMSO)_2Fe^{II}PPIX/TiO_2$ that was, within experimental error, the same. To show this clearly, the transient absorption difference spectrum obtained at 4.5 μs was subtracted from all the transient spectra collected at $t < 4.5\ \mu$s (Figure 5). This results in a difference spectrum which artificially returns to $\Delta A = 0$ at 4.5 μs. The kinetic rate constant abstracted from single-wavelength absorption changes, $[1.41(0.6)] \times 10^6\ s^{-1}$, was, within experimental error, the same as that measured after pulsed laser excitation of $(DMSO)_2Fe^{II}PPIX/TiO_2$.

At observation times longer than 4.5 μs after pulsed laser excitation of $(DMSO)(CO)Fe^{II}PPIX/TiO_2$, a second intermediate was observed with a positive ΔA from 420 to 450 nm and a bleach from 402 to 420 nm (Figure 6). The spectra were modeled as the difference between the absorption spectra for $(DMSO)(CO)Fe^{II}PPIX/TiO_2$ and $(DMSO)_2Fe^{II}PPIX/TiO_2$ (Figure 6). Comparative single-wavelength absorption changes observed after excitation of $(DMSO)(CO)Fe^{II}PPIX$ and $(DMSO)(CO)Fe^{II}PPIX/TiO_2$ are given in the Figure 6 inset. The transient

(28) Noble, R. W.; Gibson, Q. H.; Brunori, M.; Antonini, E.; Wyman, J. *J. Biol. Chem.* **1969**, *244*, 3905.
(29) Williams, G.; Watts, D. C. *Trans. Faraday Soc.* **1970**, *66*, 80.
(30) Lindsey, C. P.; Patterson, G. D. *J. Chem. Phys.* **1980**, *73*, 3348.
(31) Larsen, R. W.; Findsen, E. W. *Inorg. Chim. Acta* **1998**, *271*, 119.

Table 2. Equilibrium, Kinetic Rate Constants, and Photodissociation Quantum Yields for the Indicated Fe^{II}PPIX Carbonyl Compound

compd or material	k_{obs} or $\langle k_{KWW}\rangle$ $(s^{-1})^a$	β	k^S_{+CO} $(M^{-1}\ s^{-1})^b$	K^S_{eqCO} $(M^{-1})^c$	ϕ^d
(CO)(DMSO)Fe^{II}PPIX	265(5)	1	[2.39(0.02)] × 10^5	[1.0(0.5)] × 10^5	
(CO)(DMSO)Fe^{II}PPIX/TiO_2	460(60)	0.45(0.02)	[3.1(0.2)] × 10^5	[6(1)] × 10^4	0.55(0.01)
(CO)(py)Fe^{II}PPIX	2.0(0.2)[d]	1		[4.5(0.5)] × 10^3	
(CO)(py)Fe^{II}PPIX/TiO_2	2.2(0.3)[d]	0.68(0.06)		[2.4(0.1)] × 10^3	0.16(0.05)
(CO)(MeOH)Fe^{II}PPIX/TiO_2	[2.09(0.04)] × 10^5	1	[1.5(0.2)] × 10^7	[2.3(0.2)] × 10^5	1.00(0.03)

[a] The observed or "average" first-order rate constant measured after pulsed 532 nm excitation of the indicated compound or material in a CO-saturated solution. A β value of 1 indicates a first-order kinetic process, while a value less than unity indicates the first moment of a Levy distribution of first-order rate constants, $\langle k_{KWW}\rangle$. [b] The second-order exchange rate constant obtained from plots of k_{obs} or $\langle k_{KWW}\rangle$ versus the CO concentration. [c] The equilibrium constant for CO coordination measured at 295 K. [d] The relative quantum yield for CO release measured 10 ns after pulsed laser excitation.

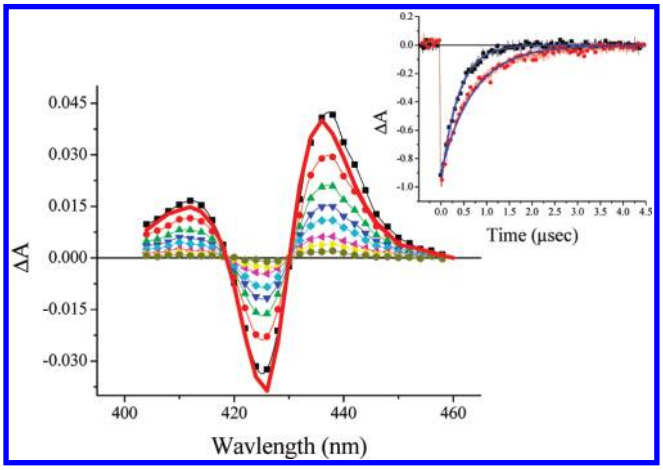

Figure 3. Transient absorption spectra measured after pulsed 532 nm laser excitation of $(DMSO)_2Fe^{II}PPIX/TiO_2$ at the following delay times: 45 ns (black squares), 0.25 μs (red circles), 0.50 μs (green triangles), 0.75 μs (blue upside-down triangles), 1.00 μs (cyan diamonds), 1.50 μs (magenta left-pointing triangles), 2.00 μs (yellow right-pointing triangles), and 4.00 μs (brown pointed circles). Overlaid is the transient absorption spectrum collected at 45 ns for $(DMSO)_2Fe^{II}PPIX$ in fluid DMSO solution (red line). The inset shows normalized single-wavelength kinetic measurements collected at 425 nm for $(DMSO)_2Fe^{II}PPIX/TiO_2$ (red circles) and $(DMSO)_2Fe^{II}PPIX$ (black squares). The data followed a first-order kinetic model with rate constants [1.35(0.03)] × 10^6 s^{-1} and [2.68(0.03)] × 10^7 s^{-1}, respectively (blue lines).

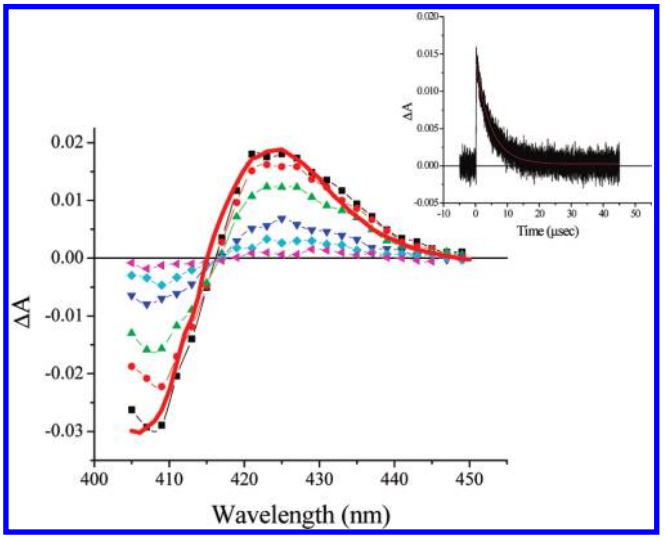

Figure 4. Transient absorption spectra measured after pulsed 532 nm laser excitation of (MeOH)(CO)$Fe^{II}PPIX/TiO_2$ at the following delay times: 0.2 μs (black squares), 1 μs (red circles), 3 μs (green triangles), 5 μs (blue upside-down triangles), 9 μs (cyan diamonds), and 10.5 μs (magenta left-pointing triangles). The data are modeled by the difference between the absorption spectra of (MeOH)(CO)$Fe^{II}PPIX/TiO_2$ and $(MeOH)_2Fe^{II}PPIX/TiO_2$, as shown by the red solid line. The inset shows single-wavelength absorption change measurements collected at 425 nm with an overlaid fit to a first-order kinetic model (red line), from which a rate constant of [2.09(0.04)] × 10^5 s^{-1} was abstracted.

data were nonexponential on TiO_2, and satisfactory fits were obtained with the KWW model (eq 3), $\langle k_{KWW}\rangle$ = 460 ± 60 s^{-1} with β = 0.45 ± 0.02 (Table 2; see also the Supporting Information). Consistent with the literature, the second intermediate exhibited single-exponential decay behavior in fluid DMSO solution with k_{obs} = 265 ± 5 s^{-1}.[17]

The dependence of the observed ligand exchange rate, k_{obs} or $\langle k_{KWW}\rangle$, on [CO] was quantified for (MeOH)(CO)$Fe^{II}PPIX/TiO_2$ and (DMSO)(CO)$Fe^{II}PPIX/TiO_2$. Transient absorption changes were monitored at the maximum growth and bleach wavelengths, for (MeOH)(CO)$Fe^{II}PPIX/TiO_2$ immersed in MeOH and (DMSO)(CO)$Fe^{II}PPIX/TiO_2$ immersed in DMSO over a [CO] range from 0 to 1.08 × 10^{-2} M or 1.1 × 10^{-3} M, respectively. A plot of $\langle k_{KWW}\rangle$ versus [CO] for (DMSO)(CO)$Fe^{II}PPIX/TiO_2$ is shown in the Figure 7 inset, from which the second-order rate constant for ligand exchange, k^{DMSO}_{+CO}, was calculated: [3.1(0.2)] × 10^5 M^{-1} s^{-1}. Similar analysis for (MeOH)(CO)$Fe^{II}PPIX/TiO_2$ was conducted, and k^{MeOH}_{+CO} was found to be [1.5(0.2)] × 10^7 M^{-1} s^{-1}. The observed exchange rate for (py)(CO)$Fe^{II}PPIX/TiO_2$ in pyridine did not vary linearly with the CO concentration.

The relative quantum yields, ϕ, for the photorelease of CO from (L)(CO)$Fe^{II}PPIX/TiO_2$ in DMSO, pyridine, and MeOH were recorded 10 ns after pulsed 532 nm excitation. The absorbance of each sample was matched at the excitation wavelength, and the laser irradiance was held at a constant value of 3 mJ/pulse such that < 1 mJ of light was absorbed per pulse. Under these conditions the quantum yields were found to be dependent on the solvent. The yields were quantified relative to (MeOH)(CO)$Fe^{II}PPIX/TiO_2$, assigned ϕ = 1 (Table 2), and increased in the order L = py < DMSO < MeOH.

Discussion

Thin films comprised of ~20 nm anatase TiO_2 nanocrystallites interconnected in a ~10 μm mesoporous (~50%) layer have received considerable attention for solar energy conversion applications.[10] Such materials are now commercially available from two different sources.[32,33] The

(32) Dyesol, http://www.dyesol.com.
(33) Solaronix, http://www.solaronix.com/.

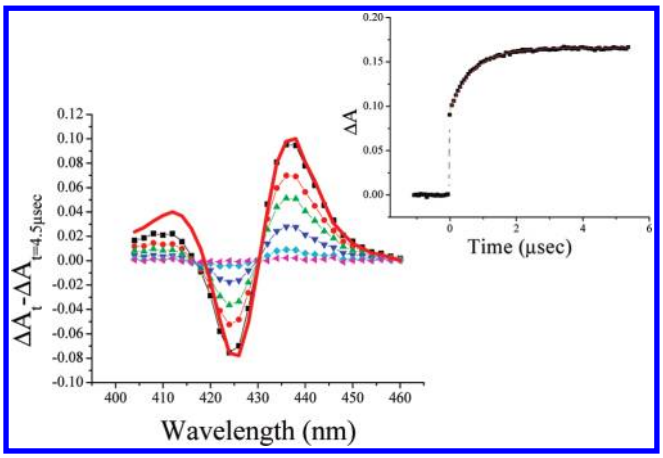

Figure 5. Transient absorption difference spectra were measured after pulsed 532 nm light excitation of (DMSO)(CO)Fe^{II}PPIX/TiO_2 immersed in CO-saturated DMSO solution, and the spectrum collected at $t = 4.5\,\mu s$ was subtracted from the spectra shown that were recorded at the following delay times: 45 ns (black squares), 0.25 μs (red circles), at 0.5 μs (green triangles), 1.0 μs (blue upside-down triangles), 2.0 μs (cyan diamonds), and 4.0 μs (magenta left-pointing triangle). Overlaid is the transient absorption spectrum collected 45 ns after 532 nm pulsed-light excitation of $(DMSO)_2Fe^{II}PPIX/TiO_2$ (red line). The inset shows single-wavelength kinetic measurements collected at 425 nm for (DMSO)(CO)Fe^{II}PPIX/TiO_2. The data followed a first-order kinetic model with an observed rate of $[1.41(0.6)] \times 10^6\ s^{-1}$ (red line).

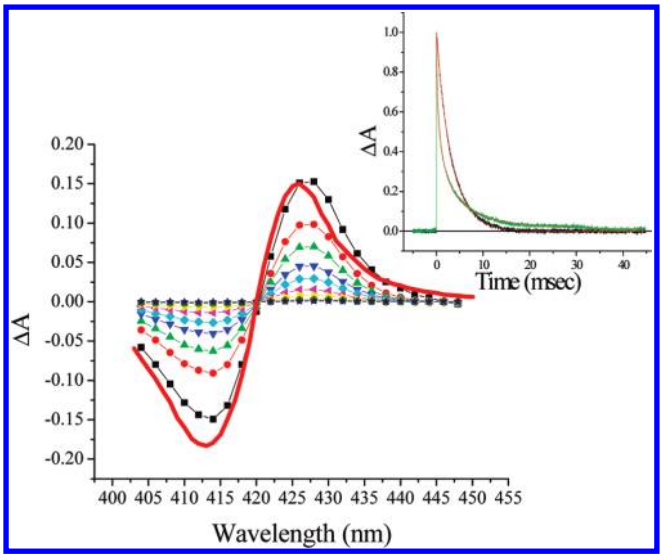

Figure 6. Transient absorption spectra observed after pulsed 532 nm light excitation of (DMSO)(CO)Fe^{II}PPIX/TiO_2 immersed in CO-saturated DMSO at $t = 4.5\,\mu s$ (black squares), 0.5 ms (red circles), 1.0 ms (green triangles), 2.0 ms (blue upside-down triangles), 4.0 ms (cyan diamonds), 8.0 ms (magenta left-pointing triangles), 12 ms (yellow left pointing triangles), 20 ms (brown pointed circles), and 28 ms (navy stars). The data are modeled by the $(DMSO)_2Fe^{II}PPIX/TiO_2$ and (DMSO)(CO)Fe^{II}PPIX/TiO_2 absorption difference spectrum (red line). The inset shows comparative single-wavelength kinetic data collected at 428 nm for (DMSO)(CO)Fe^{II}PPIX/TiO_2 (green) and (DMSO)(CO)-Fe^{II}PPIX (black) in fluid solution. Overlaid are the fits to appropriate kinetic models (red lines). The (DMSO)(CO)Fe^{II}PPIX data follow a first-order kinetic model with the observed rate constant of 265(5) s^{-1}. The (DMSO)(CO)Fe^{II}PPIX/TiO_2 data are fit to the KWW function, resulting in an average observed rate constant, $\langle k_{KWW} \rangle = 460(60)\ s^{-1}$.

mesopores allow transition-metal catalysts and reactants to diffuse throughout them, and the high surface area enables a large number of catalysts to be anchored within a small

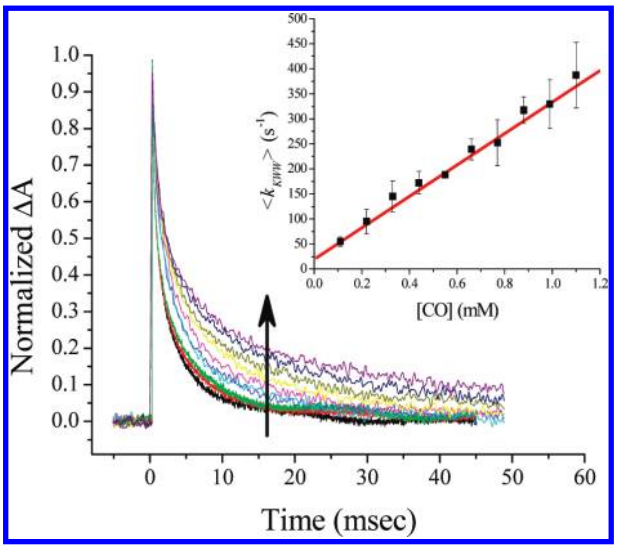

Figure 7. Normalized single-wavelength absorption changes monitored at 428 nm after pulsed 532 nm light excitation of (DMSO)(CO)Fe^{II}PPIX/TiO_2 in DMSO as a function of the CO concentration: 1.1 mM (black), 0.99 mM (red), 0.88 mM (green), 0.77 mM (blue), 0.66 mM (cyan), 0.55 mM (magenta), 0.44 mM (yellow), 0.33 mM (brown), 0.22 mM (navy), and 0.11 mM (purple). The arrow gives the direction of decreased CO concentration. The inset shows the dependence of $\langle k_{KWW} \rangle$ on [CO], where the errors bars indicate the standard deviation obtained from the average of three separate measurements. The slope was $(3.1 \pm 0.2) \times 10^5\ M^{-1}\ s^{-1}$.

geometric area.[10] In agreement with previous work, the hemes were found to bind strongly to the anatase particles with an equilibrium constant of $\sim 10^5\ M^{-1}$ and saturation surface coverages of 10^{-8} mol/cm^2.[26] The two carboxylic acid groups are a key to surface binding, and a heme without such groups, i.e. iron(III) *meso*-tetraphenylporphyrin chloride, showed no significant surface chemistry under the same conditions.[26] Carboxylic acid groups are in fact the most commonly utilized, and vibrational spectroscopy experiments have shown that they are present on TiO_2 in their carboxylate form.[10] For the spectroscopic measurements in the current work, the surface concentration was intentionally kept a factor of 10 below saturation coverages such that approximately 30−50 porphyrins were present on each anatase nanocrystallite. The Fe(III) form was surface-anchored and photoreduced to the Fe(II) formal oxidation state as previously described.[26]

Comparative studies of the electronic absorption spectra of Fe^{II}PPIX anchored to mesoporous nanocrystalline (anatase) TiO_2 thin films with those of authentic samples in fluid solution, particularly in the Q-band region ($S_0 \rightarrow S_1$), allowed the identity of the axial ligands CO, DMSO, and pyridine to be reliably assigned and formed the basis for this study. *To a first approximation the thermodynamics and kinetics for axial ligand exchange were independent of whether the heme was dissolved in fluid solution or anchored to a mesoporous thin film that was immersed in the same solution.* This indicates that surface binding had only a minor influence on heme coordination chemistry. The axial ligands were quantitatively exchanged by introduction of the alternative ligands into the mesopores of the thin film. While this finding may not be entirely surprising, the accessibility of surface-confined molecules to other molecules present in the mesopores is otherwise difficult to address experimentally. Previous studies with solvatochromic probes, such as $Ru(dcb)(CN)_4^{2-}$, where dcb is 4,4′-$(COOH)_2$-2,2′-bipyridine, have also shown

Scheme 3. Dissociative Mechanism for CO and DMSO Ligand Exchange

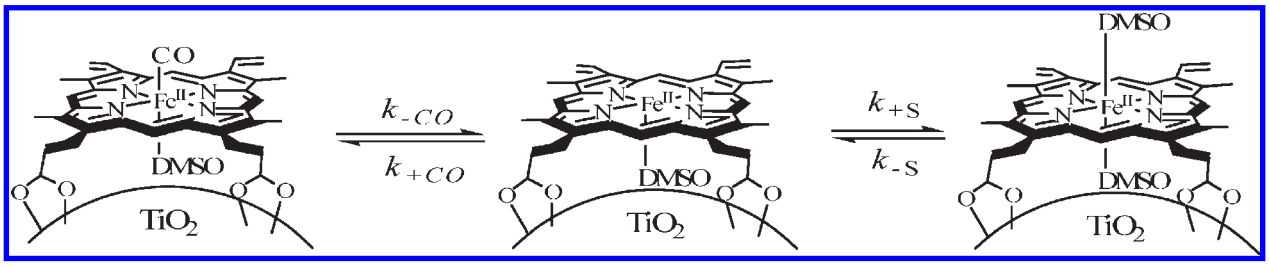

that the surface-bound molecules were well-solvated, but the broad metal-to-ligand charge-transfer (MLCT) absorption bands observed made quantitative analysis difficult.[34] Here it is clear that within experimental uncertainty all hemes were accessible to ligands present in the mesopores and the thermodynamics and kinetics for coordination chemistry could be quantified with signal-to-noise ratios very comparable to those in fluid solution.

There were, however, two small yet significant changes to the coordination chemistry when the hemes were surface-confined within the mesoporous thin films and immersed in pyridine or DMSO: (1) the equilibrium constant for CO coordination decreased by about a factor of 2 and (2) the appearance of complex nonexponential ligand exchange kinetics. Interestingly, the kinetics for CO exchange were first order when CO-saturated methanol was present in the mesopores, but the poor solubility of heme in methanol precluded comparative studies. Absent was any clear evidence for excited-state electron injection into TiO_2 that might have been expected. The remainder of this discussion is focused on understanding these behaviors.

The equilibrium constants measured for CO coordination to hemes anchored to TiO_2 increased in the order py < DMSO < MeOH, a trend dictated by the strength of the Fe−solvent bond and one that could have been predicted on the basis of the previous studies of Brault and Larsen.[17,35] In both DMSO and py, this equilibrium constant was about a factor of 2 larger than the corresponding value measured in solution. Interestingly, previous comparative studies of halide coordination to Zn(II) porphyrins also showed a factor of 2 decrease in equilibrium constants when the metalloporphyrin was anchored to TiO_2.[36]

There exists an impressive body of data that indicates a dissociative mechanism for ligand exchange in hemes. A five-coordinate heme intermediate is therefore expected (Scheme 3).[28,37] In fact, hemes were selected for this study, as the mechanism of ligand exchange has been exhaustively studied under many experimental conditions.[11−15]

The equilibrium constant for CO binding is defined by the elementary steps in a D mechanism (eq 5), and is influenced by the kinetics of both CO and solvent coordination and dissociation. The factor of two smaller equilibrium constant measured on the TiO_2 surface may reflect that only one face of the heme is available for CO/solvent release and binding, as is suggested in Scheme 3. The question then arises as to how the TiO_2 environment might influence the kinetics for solvent *and* CO exchange.

$$K^{S}_{eqCO} = \frac{k_{-S}k_{+CO}}{k_{+S}k_{-CO}} \quad (5)$$

To gain some insight into this question, pulsed laser excitation was used to photorelease CO and/or DMSO ligands. The rate of return to the equilibrium state was then quantified by nanosecond transient absorption spectroscopy. This is the standard "flash and trap" approach pioneered by Gibson for the study of dioxygen activation by hemes.[28] In fluid solution, the observed kinetics were first order, in agreement with many previous studies.[38] In proteins and heterogeneous media, nonexponential kinetics have been reported and the same was observed here after pulsed light excitation of (S)(CO)Fe^{II}PPIX/TiO_2 where S is pyridine or DMSO. In agreement with previous studies of hemes in proteins, the observed kinetics were well described by the Kohlrausch−Williams−Watts (KWW) function.[39−43]

While the origin of the nonexponential kinetics for CO equilibration within the mesopores of the TiO_2 thin film is not known, there has been much discussion of such kinetic mechanisms in biological media.[39−43] The discovery some time ago, that geminate recombination of photoreleased CO and heme present in myoglobin and hemoglobin occurred on nanosecond and longer time scales, has invoked much speculation of the underlying cause.[39−45] Slow geminate recombination suggested that the photoreleased CO was trapped at different locations within the protein and recombination occurred from a distribution of distances, resulting in a distribution of barrier heights and hence rate constants.[43,44] Similar behavior could occur within the TiO_2 mesopores, and there is some evidence to support this. First, the quantum yields for CO photorelease were less than unity, indicating that significant geminate recombination occurred within 10 ns, behavior that to our knowledge has no precedence in fluid solution.[39−42,45] The quantum yield of photoinduced CO loss in myoglobin is known to be unity.[11,45] Additionally, CO is

(34) Argazzi, R.; Bignozzi, C. A.; Yang, M.; Hasselmann, G. M.; Meyer, G. J. *Nano Lett*. **2002**, *2*, 625.
(35) Brault, D.; Rougee, M. *Biochemistry* **1974**, *13*, 4591.
(36) Morris, A. J.; Marton, A.; Meyer, G. J. *Inorg. Chem*. **2008**, *47*, 7681.
(37) Kadish, K. M. *Database of Redox Potentials and Binding Constants*; Academic Press: San Diego, CA, 1999; Vol. *9*.
(38) Traylor, T. G. *Acc. Chem. Res*. **1981**, *14*, 102.
(39) Nienhaus, G. U.; Mourant, J. R.; Chu, K.; Frauenfelder, H. *Biochemistry* **2002**, *33*, 13413.
(40) Steinbach, P. J.; Ansari, A.; Berendzen, J.; Braunstein, D.; Chu, K.; Cowen, B. R.; Ehrenstein, D.; Frauenfelder, H.; Johnson, J. B. *Biochemistry* **2002**, *30*, 3988.
(41) Frauenfelder, H.; Alberding, N. A.; Ansari, A.; Braunstein, D.; Cowen, B. R.; Hong, M. K.; Iben, I. E. T.; Johnson, J. B.; Luck, S. *J. Phys. Chem*. **2002**, *94*, 1024.
(42) Plonka, A. *Chem. Phys. Lett*. **1988**, *151*, 466.
(43) Berlin, Y. A.; Fischer, S. F.; Goldanskii, N. I. C. V. I. *Chem. Phys*. **1995**, *200*, 369.
(44) (a) Reynolds, A. H.; Rand, S. D.; Rentzepis, P. M. *Proc. Natl. Acad. Sci. U.S.A*. **1981**, *78*, 2292. (b) Agmon, N.; Hopfield, J. J. *J. Chem. Phys*. **1983**, *79*, 2042.
(45) Ye, X.; Demidov, A.; Champion, P. M. *J. Am. Chem. Soc*. **2002**, *124*, 5914.

known to bind to TiO_2.[46] The possibility that a distribution of such adducts are the CO source that denotes to the five-coordinate heme is not unreasonable.[46] The appearance of first-order kinetics for recombination in methanol would then imply that CO is more effectively solvated by methanol and that the putative TiO_2-CO adducts are not present in this solvent. This would account for the much higher yield for CO photorelease measured on a nanosecond time scale in methanol.

Inverse Laplace transform of the KWW function reveals an underlying Levy distribution of first-order rate constants.[30,47] This distribution is analytically known for discrete values of β and has been estimated by saddle-point and other approximations for all positive values of β less than unity.[47] When β is equal to 1, the KWW function reduces to a first-order kinetic model. As β values decrease from unity, a broad and more highly skewed distribution of first-order rate constants results.[30,47] The values for CO coordination in DMSO ($\beta = 0.45 \pm 0.02$) and pyridine ($\beta = 0.68 \pm 0.06$) correspond to distributions that have significant amplitudes on time scales from picoseconds to milliseconds. The lower β values abstracted from data obtained in DMSO reflects a higher degree of heterogeneity that may indicate different coordination modes of the DMSO ligand (see below). The first-order behavior observed in methanol indicates homogeneous coordination chemistry like that reported previously for hemes in fluid solution.[38] We note that an "average" rate constant, $\langle k_{KWW} \rangle$, is often quantified on the basis of the first moment of the KWW function, as was done here.

The second-order exchange rate constant, k^S_{+CO}, was determined by quantifying k_{obs} or $\langle k_{KWW} \rangle$ as a function of [CO] (eq 6). This equation predicts that the intercept would yield information on the rate constant for CO dissociation; however, systematic studies by Traylor and others have shown that this does not provide reliable rate constants.[38]

$$k_{obs} = k^S_{+CO}[CO] + k^S_{-CO} \quad (6)$$

With regard to Scheme 3, k^S_{+CO} is equal to $k_{+CO}k_{-S}/k_{+S}[S]$, as dictated by Gibson.[28] The k^S_{+CO} values abstracted from data acquired after pulsed laser excitation of (DMSO)(CO)Fe^{II}-PPIX/TiO_2 were 30% larger (i.e., 3.1×10^5 M^{-1} s^{-1} vs 2.39×10^5 M^{-1} s^{-1}) than (DMSO)(CO)Fe^{II}PPIX in fluid solution. Interestingly, the corresponding exchange rate for CO coordination to $(py)_2Fe^{II}$PPIX/TiO_2 was independent of the CO concentration, indicating that pyridine dissociation was rate-limiting.

Light excitation of the bis-solvated hemes in methanol or pyridine did not result in a measurable absorption change on nanosecond or longer time scales, indicating that either the ligands were not photoreleased or that they recombined within the ~10 ns time resolution of the instrumentation utilized. Given that a ligand field state which is antibonding with respect to metal−ligand bonds is known to be rapidly populated after $\pi-\pi^*$ excitation of hemes, the latter interpretation is favored.[48] Pulsed light excitation of $(DMSO)_2Fe^{II}$PPIX, on the other hand, did lead to the appearance of a long-lived intermediate. The spectral features of this transient and the measured kinetics were in good agreement with a previous study where a high-spin, five-coordinate heme was proposed, (DMSO)Fe^{II}PPIX.[25,27] In neat DMSO, the ligation of a second DMSO molecule was surprisingly slow ($k = 2.7 \times 10^7$ s^{-1}) and the rate constant was a factor of 20 lower when the heme was anchored to TiO_2 ($k = 1.35 \times 10^6$ s^{-1}). This same putative five-coordinate intermediate was observed spectroscopically after pulsed laser excitation of (DMSO)(CO)Fe^{II}PPIX both in fluid solution and within the TiO_2 thin films. If a spin change does indeed create a significant barrier for DMSO coordination and the observed rate constant reflects k_{+S} in Scheme 3 and is the only rate constant sensitive to the TiO_2 environment, an increased equilibrium constant for CO coordination would result, contrary to what was observed. Therefore, the decreased value of k_{+DMSO} measured upon surface immobilization would have to be accompanied by an increase in the CO off-rate and/or increases in the rate constants for CO coordination or solvent dissociation (eq 5).

An alternative explanation for the long-lived transient observed after pulsed laser excitation of (DMSO)Fe^{II}PPIX in DMSO exists. The coordination geometry of the coordinated DMSO may change with light perturbation. Rack and co-workers have demonstrated linkage photoisomerization, Ru−S and Ru−O, of Ru^{II} and Os^{II} DMSO compounds, and similar isomers have been proposed for iron porphyrinates as well as Pt and Pd compounds.[49−52] It may therefore be that a DMSO linkage isomer was created with light rather than the proposed five-coordinate heme.

The lack of efficient excited-state injection into TiO_2 is in itself of interest. Holten has shown that the heme excited singlet state is quenched within 1 ps by a low-lying ligand field state.[48] Excited-state injection has been shown to occur on this or even faster time scales under some conditions.[53−63] The heme excited states are only weakly electronically coupled to the semiconductor surface, due to the sp^3-hybridized carbons in the ethylene chain that separate the porphyrin ring from the carboxylic acid binding groups. Lian and Mohler have shown that the average excited-state

(46) Yates, D. J. C. *J. Phys. Chem.* **1961**, *65*, 746.
(46) Yates, D. J. C. *J. Phys. Chem.* **1961**, *65*, 746.
(47) Majumdar, C. K. *Solid State Commun.* **1971**, *9*, 1087.
(48) Dixon, D. W.; Kirmaier, C.; Holten, D. *J. Am. Chem. Soc.* **1985**, *107*, 808.
(49) Ducommun, Y.; Merbach, A. E.; Hellqvist, B.; Elding, L. I. *Inorg. Chem.* **2002**, *26*, 1759.
(50) Hu, C.; Noll, B. C.; Scheidt, W. R. *Inorg. Chem.* **2007**, *46*, 8258.
(51) Rachford, A. A.; Rack, J. J. *J. Am. Chem. Soc.* **2006**, *128*, 14318.
(52) Rack, J. J.; Winkler, J. R.; Gray, H. B. *J. Am. Chem. Soc.* **2001**, *123*, 2432.
(53) Tachibana, Y.; Moser, J. E.; Gratzel, M.; Klug, D. R.; Durrant, J. R. *J. Phys. Chem.* **1996**, *100*, 20056.
(54) Hannappel, T.; Burfeindt, B.; Storck, W.; Willig, F. *J. Phys. Chem. B* **1997**, *101*, 6799.
(55) Heimer, T. A.; Heilweil, E. J. *J. Phys. Chem. B* **1997**, *101*, 10990.
(56) Heimer, T. A.; Heilweil, E. J.; Bignozzi, C. A.; Meyer, G. J. *J. Phys. Chem. A* **2000**, *104*, 4256.
(57) Ellingson, R. J.; Asbury, J. B.; Ferrere, S.; Ghosh, H. N.; Sprague, J. R.; Lian, T.; Nozik, A. J. *J. Phys. Chem. B* **1998**, *102*, 6455.
(58) Piotrowiak, P.; Galoppini, E.; Wei, Q.; Meyer, G. J.; Wiewior, P. *J. Am. Chem. Soc.* **2003**, *125*, 5278.
(59) Benko, G.; Kallioinen, J.; Korppi-Tommola, J. E. I.; Yartsev, A. P.; Sundstrom, V. *J. Am. Chem. Soc.* **2002**, *124*, 489.
(60) Benko, G.; Myllyperkio, P.; Pan, J.; Yartsev, A. P.; Sundstrom, V. *J. Am. Chem. Soc.* **2003**, *125*, 1118.
(61) Kallioinen, J.; Benko, G.; Sundstrom, V.; Korppi-Tommola, J. E. I.; Yartsev, A. P. *J. Phys. Chem. B* **2002**, *106*, 4396.
(62) Kuciauskas, D.; Monat, J. E.; Villahermosa, R.; Gray, H. B.; Lewis, N. S.; McCusker, J. K. *J. Phys. Chem. B* **2002**, *106*, 9347.
(63) Asbury, J. B.; Hao, E.; Wang, Y.; Ghosh, H. N.; Lian, T. *J. Phys. Chem. B* **2001**, *105*, 4545.

injection rate constants for compounds of the type Re(bpy−$(CH_2)_n$−$CO_2H)_2(CO)_3Cl$ decrease markedly with increased n.[64,65] Excited-state injection for a methylene spacer and propylene spacer occurred with injection rates of 19 and 240 ps^{-1} that are much slower than the ligand field deactivation reported by Holten.[65] Therefore, on the basis of these data one would not anticipate efficient excited-state injection for these hemes, and none was observed.

Conclusions

Systematic and comparative studies of CO equilibrium and ligand exchange dynamics for hemes in fluid solution and anchored to mesoporous nanocrystalline (anatase) TiO_2 thin films immersed in the same solvent have been conducted. To a first approximation, heme coordination chemistry was remarkably insensitive to the TiO_2 environment. Small but significant influences of the mesoporous nanocrystalline TiO_2 environment were manifest by the appearance of complex kinetics and a factor of 2 decrease in the equilibrium constant for CO coordination relative to fluid solution. The kinetics were well described by the Kohlrausch−Williams−Watts model that has previously been utilized to quantify ligand exchange dynamics of hemes in proteins. A distribution of distances between five-coordinate hemes and CO within the TiO_2 mesopores was proposed to underlie the nonexponential kinetics. Rapid "geminate" recombination of photoreleased CO resulted in less than unity quantum yields for CO photorelease measured on nanosecond time scales. A kinetic analysis based on the well-established dissociative mechanism for heme ligand exchange suggested that the smaller equilibrium constants for CO−heme coordination within the TiO_2 mesopores resulted from enhanced CO dissociation rate constants and/or smaller solvent concentrations within the mesopores. CO dissociation and/or smaller rate constants for solvent dissociation. Absent from the heme excited-state chemistry was evidence of excited-state injection into the anatase nanocrystallites. Rapid internal conversion from the porphyrin singlet state to dissociative ligand field states was proposed to inhibit excited-state injection, behavior that was promoted by the ethylene spacer between the porphyrin ring and the carboxylic acid anchoring groups.

AcknowledgmentAcknowledgment. is made to the donors of the Petroleum Research Fund, administered by the American Chemical Society, and to the National Science Foundation for support of this research.

Supporting Information Available: Figures giving additional kinetic data and absorption spectra. This material is available free of charge via the Internet at http://pubs.acs.org.

(64) Anderson, N. A.; Ai, X.; Chen, D.; Mohler, D. L.; Lian, T. *J. Phys. Chem. B* **2003**, *107*, 14231.
(65) Asbury, J. B.; Hao, E.; Wang, Y.; Lian, T. *J. Phys. Chem. B* **2000**, *104*, 11957.